Coordination Chemistry

Tailored Transition-Metal Coordination Environments in Imidazole-Modified DNA G-Quadruplexes

Philip M. Punt and Guido H. Clever*[a]

Abstract: Two types of imidazole ligands were introduced both at the end of tetramolecular and into the loop region of unimolecular DNA G-quadruplexes. The modified oligonucleotides were shown to complex a range of different transition-metal cations including Ni[II], Cu[II], Zn[II] and Co[II], as indicated by UV/Vis absorption spectroscopy and ion mobility mass spectrometry. Molecular dynamics simulations were performed to obtain structural insight into the investigated systems. Variation of ligand number and position in the loop region of unimolecular sequences derived from the human telomer region (htel) allows for a controlled design of distinct coordination environments with fine-tuned metal affinities. It is shown that Cu[II], which is typically square-planar coordinated, has a higher affinity for systems offering four ligands, whereas Ni[II] prefers G-quadruplexes with six ligands. Likewise, the positioning of ligands in a square-planar versus tetrahedral fashion affects binding affinities of Cu[II] and Zn[II] cations, respectively. Gaining control over ligand arrangement patterns will spur the rational development of transition-metal-modified DNAzymes. Furthermore, this method is suited to combine different types of ligands, for example, those typically found in metalloenzymes, inside a single DNA architecture.

Introduction

In the biological world, transition metals are key players in countless central processes ranging from structural stabilization over electron transport and oxygen metabolism to enzyme catalysis.[1] Which metal suits which function largely depends on its redox properties, accessible spin states and Lewis acidity/basicity. Embedded in a protein environment, these properties are fine-tuned by structurally defined and highly conserved coordination spheres, typically consisting of proteinogenic amino acid side chains and backbones.[2]

The first shells of biological coordination sites usually share some of the following principles: 1) controlled number of donors 2) their precise, 3-dimensional positioning around the metal cation, 3) heteroleptic donor combinations, and 4) mixtures of weaker and stronger coordinating ligands.[3] Often neglected, however, is a thorough discussion of the second coordination sphere, which is in fact no less important than the first shell. It is involved in shaping the geometry of the active site and fine-tuning the electronic environment. It may further control substrate and product transport, selectivity, proton-shuttling through channels, electron transport and many further processes.[3, 4]

In this respect, the synthetic branch of bioinorganic chemistry usually investigates the design and synthesis of chelating coordination environments, often podands or macrocycles, meant to resemble the first coordination sphere found within metalloproteins and other metal-binding biopolymers. A classical approach to mimic such coordination environments is the tedious multistep synthesis of chelate ligands and corresponding model complexes. Improving or modifying the structure and function of these coordination compounds requires a laborious variation of donor site number, position and chemistry, if no modular approach can be chosen.[5]

A different strategy to tackle this issue is to follow closer the natural pattern and utilize peptides or proteins to design defined coordination environments. Therefore, natural protein scaffolds can be covalently or noncovalently modified with catalytically active metal complexes, even those that do not occur in nature. Alternatively, de novo designed folding motifs—typically alpha helices and beta barrels—are synthesized and connected to arrange ligating amino acid side chains in the desired way around a metal binding site. A related strategy builds on reducing a natural metalloprotein to its minimal functional unit by removing all parts not mandatory for its function.[6]

This concept cannot be applied only to proteins but also to other biopolymers including nucleic acids. Transition-metals have been embedded into nucleic acid structures by the non-/covalent attachment of chelate ligands. Examples include cerium complexes acting as sequence-specific DNA cleavers,

[a] P. M. Punt, Prof. Dr. G. H. Clever
Faculty of Chemistry and Chemical Biology, TU Dortmund University
Otto-Hahn-Straße 6, 44227 Dortmund (Germany)
E-mail: guido.clever@tu-dortmund.de

palladium complexes for the generation of singlet oxygen, Cu[II]-complexes for the enantioselective catalysis of Friedel–Crafts reactions, Michael Additions, sulfoxidations or *syn* hydrations.[7]

In contrast to these embedding strategies, the field of metal-mediated base pairing studies metal coordination as replacement of the canonical Watson–Crick hydrogen bonds.[8] Previously, this concept was mostly applied in duplex DNA and only a limited number of articles reported about metal-mediated base interaction in higher secondary structures.[9] Examples include metal-coordinating triplex DNA,[9a] i-motifs[9b] and G-quadruplex structures.[9c] The latter ones assemble from guanine-rich sequences, in which four guanine residues form planar G-tetrads through circular Hoogsteen base pairing. Under incorporation of central monovalent cations, typically Na^{+} or K^{+}, the tetrads stack via π–π interactions to give G-quadruplexes.[10]

Recently, our group was the first to report an example of a transition-metal-binding G-quadruplex in which one of the G-tetrads was replaced by four pyridine ligands, allowing for the complexation of Cu[II] and Ni[II] cations.[9c] This concept was employed to realize the Cu[II]-triggered inhibition of thrombin via a specific quadruplex aptamer, a molecular EPR ruler (with two copper centers acting as spin labels) and a Cu[II]-switchable peroxidase mimic consisting of a DNA G-quadruplex adduct with hemin.[11, 12a]

Inspired by the natural amino acid histidine, we herein report the incorporation of a new imidazole-based ligand into tetra and unimolecular G-quadruplexes.[12] Although the inclusion in tetramolecular G-quadruplexes offer only limited control of ligand number (multiples of four) and arrangement (3′ and/or 5′ end),[11, 12a, 13] we herein show that unimolecular G-quadruplexes present a highly robust system to vary the position and number of incorporated ligands. We present how this approach allows us to fine-tune the coordination environment of different transition-metal cations with respect to their preferred coordination number and geometry. This further enables the design of systems with coordinatively unsaturated metal centers, being potentially attractive for applications in catalysis. Gaining high control over the construction of specific coordination environments by a straightforward DNA sequence design represents a fundamental prerequisite on the way to develop new DNA-based metalloenzyme mimics.

Results and Discussion

For our study, the previously reported[12a] imidazole-based ligand L[1] and its derivative L[2], which bears an additional ethanol linker, were incorporated in both of their enantiomeric forms (L[1R/S], L[2R/S]) into a number of tetramolecular and unimolecular G-quadruplex sequences. The phosphoramidites needed for solid-phase synthesis were accessed according to procedures reported before.[12a] An initial nucleophilic ring opening of DMT-protected (R/S)-glycidol (DMT = 4,4′-dimethoxytrityl) was followed by a phosphorylation reaction to access phosphoramidite building blocks. Both stereoisomers with either R- or S-configuration at the carbon in the branching po-
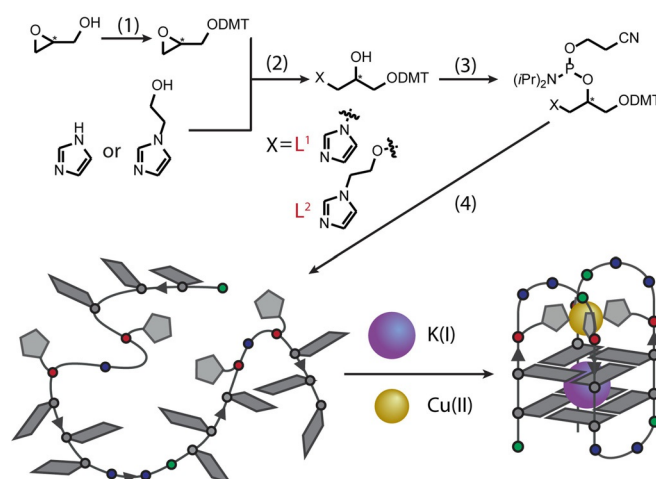

Figure 1. Synthesis of imidazole ligands L[1] and L[2]. (1) DMT-Cl, glycidol and Et$_3$N in CH$_2$Cl$_2$, (2) L[1]: imidazole and DMT-glycidin in 1,4-dioxane at 80 °C or L[2]: 1-(2-hydroxyethyl)imidazole, DMT-glycidol and NaH in DMF at 40 °C, (3) CEDIP-Cl, imidazole derivative and DIPEA in CH$_2$Cl$_2$ at rt, (4) DNA solid phase synthesis. DIPEA = N,N-diisopropylethylamine; CEDIP-Cl = 2-cyanoethyl N,N-diisopropylchlorophosphoramidite.

sition were prepared (Figure 1). DNA solid-phase synthesis was performed according to standard protocols (Supporting Information). Coupling times for L[1] and L[2] were extended to maximize coupling efficiencies which were usually > 99 % per coupling. After solid-phase synthesis, DNA samples were deprotected in aqueous ammonia at 55 °C and purified in "DMT-on" mode by using reversed-phase HPLC. After purification, the final DMT-group was removed by using C18-Sepak cartridges and aqueous TFA (2 %).

G-quadruplex formation was characterized by UV/Vis-based melting experiments, thermal difference spectra (TDS), CD spectroscopy and mass spectrometry. In the case of melting experiments, a temperature-dependent change of absorption at 295 nm was observed, which is characteristic for G-quadruplex denaturation/renaturation.

Incorporation of L[1] or L[2] at the 5′ terminal position of tetramolecular G-quadruplex G$_4$L resulted in the formation of a parallel strand arrangement as indicated by CD spectroscopy, showing a characteristic positive Cotton effect at approximately 264 nm (Figure 2). An additional maximum could be observed at 295 nm, the origin of which is still under debate.[13] Thermal denaturation experiments revealed a slightly higher stability for G$_4$L[2] [T_m(G$_4$L[2R]) = 34 °C, T_m(G$_4$L[2S]) = 36 °C; T_m = melting temperature] compared to G$_4$L[1] (T_m(G$_4$L[1R]) = 32 °C, T_m(G$_4$L[1S]) = 31 °C). In line with our previous observations, this effect could be explained by the longer linker of L[2] that facilitates better π-stacking of the imidazole moieties with the upper G-tetrad, contributing to a higher thermal stability.[13] Subsequently, transition-metal binding was investigated. In accordance with our previously reported results for L[1], the L[2]-modified G-quadruplexes G$_4$L[2R] and G$_4$L[2S] were observed to complex Cu[II], Ni[II], Zn[II] and Co[II][14] cations as indicated by strong thermal stabilization effects (Table 1; Supporting Information, Table S3) by retaining the all-parallel topology. All sequences were found to bind one equivalent of the respective metal
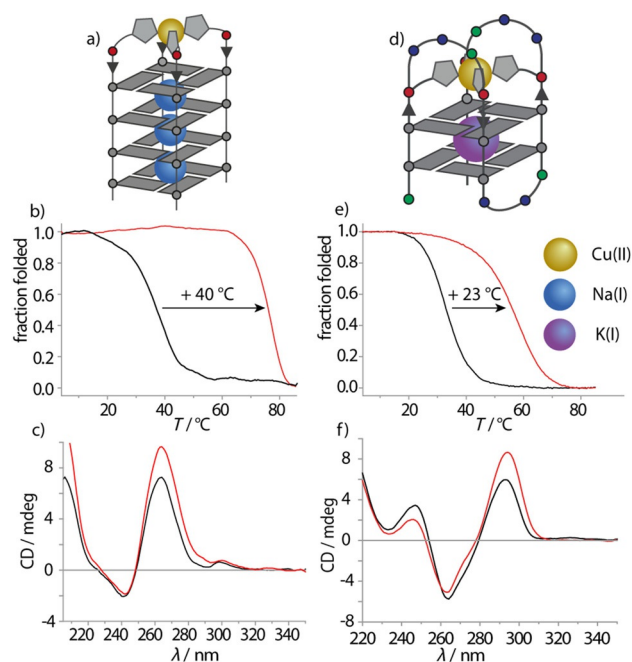
Figure 2. a) Schematic representation of G₄L in complex with Cuᴵᴵ, b) thermal denaturation spectra of G₄L²ˢ before (black) and after (red) Cuᴵᴵ addition, c) CD spectra of G₄L²ˢ before (black) and after (red) Cuᴵᴵ addition, d) schematic representation of htelL₄, e) thermal denaturation spectra of htelL²ˢ₄ before (black) and after (red) Cuᴵᴵ addition, f) CD spectra of htelL²ˢ₄ before (black) and after (red) Cuᴵᴵ addition. Samples were prepared in 100 mм NaCl (tetramolecular) or KCl (unimolecular), 10 mм LiCaCo pH 7.2 and 0.94 or 1.88 µм Cuᴵᴵ (tetramolecular and unimolecular, respectively) at G-quadruplex concentrations of 3.75 µм (tetramolecular) and 1.875 µм (unimolecular).

Table 1. Melting temperatures T_m (and ΔT_m) of unimolecular and tetramolecular G-quadruplexes, respectively, in absence and presence of different transition metal cations. Conditions: 3.75 (tetramolecular) and 1.88 µм (unimolecular) ssDNA in 100 mм NaCl (tetramolecular) or KCl (unimolecular), unless stated differently; 10 mм LiCaCo pH 7.2 and, if present, 1 equiv transition-metal cations (with respect to the folded G-quadruplex). "No metal" refers to the absence of transition-metal cations.

	No metal	Cuᴵᴵ	Niᴵᴵ	Znᴵᴵ	Coᴵᴵ
G₄L¹ˢ	31	79 (+48)	77 (+46)	54 (+23)	64 (+33)
G₄L²ˢ	36	76 (+40)	73 (+37)	52 (+16)	63 (+27)
htelL¹ˢ₄	37	36 (−1)	36 (−1)	36 (−1)	37 (+0)
htelL²ˢ₂B[a]	53	55 (+2)	53 (+0)	54 (+1)	53 (+0)
htelL²ˢ₃B[a]	50	56 (+6)	51 (+1)	52 (+2)	50 (+0)
htelL²ˢ₄	33	56 (+23)	45 (+12)	36 (+3)	35 (+2)
htelL²ˢ₅	33	54 (+21)	55 (+22)	37 (+4)	37 (+4)
htelL²ˢ₆	36	54 (+18)	59 (+23)	44 (+8)	44 (+8)
htelL²ˢ₇	28	43 (+15)	46 (+18)	36 (+8)	36 (+8)

[a] Measured in 100 mм NaCl.

cation, whereas the addition of further amounts resulted in no significant extra stabilization, thus indicating specific binding to the imidazole-lined cavity in a 1:1 fashion. Interestingly, G₄L² shows a higher thermal stability compared to G₄L¹ in absence of transition metals. After addition of Cuᴵᴵ, however, G₄L¹ [ΔT_m (G₄L¹ˢ) = +48 °C, ΔT_m (G₄L¹ᴿ) = +51 °C] was significantly more stabilized compared to G₄L² [ΔT_m(G₄L²ᴿ) = +40 °C, ΔT_m(G₄L²ˢ) = +40 °C]. This effect can be explained by stronger

π–π interactions between L² and the neighboring G-tetrad that need to break up to facilitate metal coordination and, thus, reduce the metal-mediated thermal stabilization.[13] In addition, although for L¹ the stereochemical configuration showed an influence on the thermal stabilization, in case of L² no influence of the stereo-configuration was observed.

To further support the formation of the proposed G-quadruplex-metal complexes, native ESI-MS experiments coupled to trapped ion mobility spectrometry (TIMS) were performed. To differentiate between folded and unfolded G-quadruplexes in the gas phase, two phenomena are most instructive. First, if tetramolecular G-quadruplexes are investigated and the structure is denatured, single-stranded DNA instead of a tetramer would be observed and second, valid for tetra- and unimolecular G-quadruplexes, ESI mass spectrometry from electrolyte-containing solutions always gives rise to series of unspecific adducts with sodium or potassium cations. For fully denatured species, a statistical distribution of adducts starting with zero cations would be observed and for a native, folded species a distribution is observed starting with $n-1$ explicitly bound cations, where n is the number of G-tetrads.[15]

For G₄L²ᴿ, the analysis gave the following picture: although the quadruplex was found to be unstable in absence of Cuᴵᴵ cations, hence denatured to single strands in the gas phase, the addition of one equiv of Cuᴵᴵ led to the observation of [G₄L²ᴿK₃Cu]⁴⁻ as main species, besides a series of additional unspecific potassium adducts. Corresponding values for the TIMS-derived collisional cross-sections (CCS) (G₄L²ᴿ = 814 Å², G₄L²ˢ = 814 Å²) were comparable to reported values for unmodified G-quadruplexes.[16] Compared to the reported CCS for G₄L¹ᴿ (793 Å²), this corresponded to an increase of 21 Å², which was ascribed to the longer linker of L².[13]

Considering that we were interested in comparing CCS values of folded G-quadruplexes in the presence and absence of Cuᴵᴵ, the more stable sequence G₅L²ᴿ consisting of one additional G-tetrad was investigated. Indeed, G₅L²ᴿ was stable enough in absence of Cuᴵᴵ and the intact G-quadruplex was observed with a CCS of 868 Å² in the ESI TIMS experiment. Addition of Cuᴵᴵ resulted in a slightly larger CCS of 876 Å² (Figure 3), which was contradicting the assumption that Cuᴵᴵ coordination would "catch" freely dangling imidazole ligands resulting in a smaller CCS. However, gas-phase molecular dynamics (MD) simulations suggest that in absence of Cuᴵᴵ, the imidazole ligands lay flat on top of the G-quadruplex or in the groove regions and in presence of Cuᴵᴵ they rearrange in a more spacious propeller shape resulting in a slight increase in size (Supporting Information, Figures S85 and S86).

With promising results obtained for tetramolecular G-quadruplexes, we turned towards unimolecular G-quadruplexes. Therefore, in the human telomeric G-quadruplex sequence htel, one G-tetrad was replaced with four imidazole ligands, now called htelL₄. Investigation by CD spectroscopy, by using KCl as the electrolyte, indicated an antiparallel topology for the modification with both ligand derivatives (L¹ᴿ/ˢ and L²ᴿ/ˢ) with a positive Cotton effect at around 295 nm (Figure 2). Thermal denaturation studies of the modified G-quadruplexes showed significantly lower melting temperatures
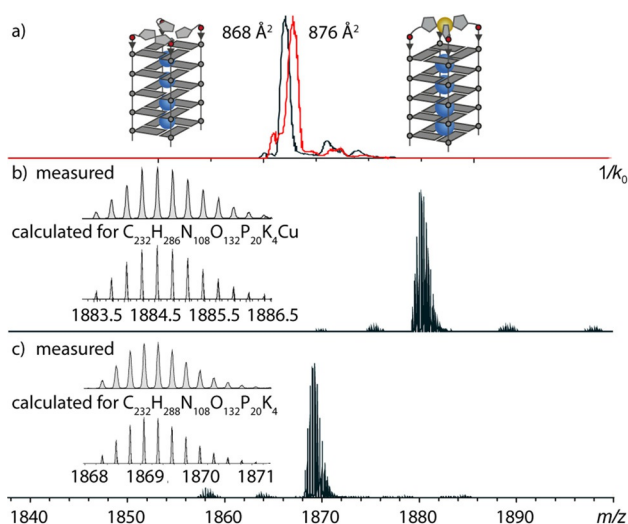
Figure 3. a) Native ESI-MS and trapped ion-mobility time-of-flight (timsTOF) experiments of G_5L^{2R} in absence and in complex with Cu^{II}. (a) Ion mobilities and corresponding collisional cross-sections. Ion-mobility-extracted mass spectra of G_5L^{2R} b) in complex with Cu^{II} and c) in absence of Cu^{II}.

$[T_m(htelL^{1S}_4) = 37\,°C$, $T_m(htelL^{2S}_4) = 33\,°C]$ compared to unmodified htel ($T_m = 64\,°C$) due to the lack of one G-tetrad.[11] Addition of different transition metals to $htelL^{1R/S}_4$ showed no signs of metal complexation, neither by CD spectroscopy nor by thermal denaturation studies. An explanation was found in the very short linker of L^1, which prevents the ligand from reaching the metal center from all four sides simultaneously and, thus, disabling metal complexation in the unimolecular system. This hypothesis was confirmed after investigating $htelL^{2R/S}_4$, which features an ethoxy-elongated linker, which was now able to complex Cu^{II}, Ni^{II}, Zn^{II} and Co^{II}. Although the addition of 1 equiv Cu^{II} ($\Delta T_m = +23\,°C$) and Ni^{II} ($\Delta T_m = +12\,°C$) to $htelL^{2S}_4$ was accompanied by a strong thermal stabilization, addition of Co^{II} ($\Delta T_m = +2\,°C$) and Zn^{II} ($\Delta T_m = +3\,°C$) resulted only in weak stabilization effects. Addition of further amounts of the respective transition metals showed no significant further increase but rather a decrease of the thermal stability, which is consistent with the specific binding of one metal cation to the imidazole modifications. Interestingly, the extent of metal-mediated thermal stabilization was highly dependent on the stereo configuration of L^2. Thus, for $htelL^{2S}_4$ higher thermal stabilizations were generally observed compared to those of its diastereomer $htelL^{2R}_4$.

To further analyze the G-quadruplex metal complexes, mass spectrometric investigations of $htelL^{2R}_4$ in the absence and presence of Cu^{II}, Ni^{II}, Zn^{II} and Co^{II} were performed. In the absence of transition metals, one main signal corresponding to the single strand was found, followed by unspecific potassium adducts, which is consistent with a denatured G-quadruplex. However, after addition of Cu^{II} and Ni^{II}, new main species corresponding to $[htelL^{2R}_4KCu]^{4-}$ and $[htelL^{2R}_4KNi]^{4-}$, respectively, were observed, consistent with natively folded G-quadruplexes. In the case of Zn^{II} and Co^{II}, the results were less clear showing a mixture of signals corresponding to denatured single strand and folded $[htelL^{2R}_4KZn]^{4-}$ or $[htelL^{2R}_4KCo]^{4-}$, respectively. This

was attributed to the lower thermal stability of the Zn^{II} and Co^{II} complexes, as compared to Cu^{II} and Ni^{II}.
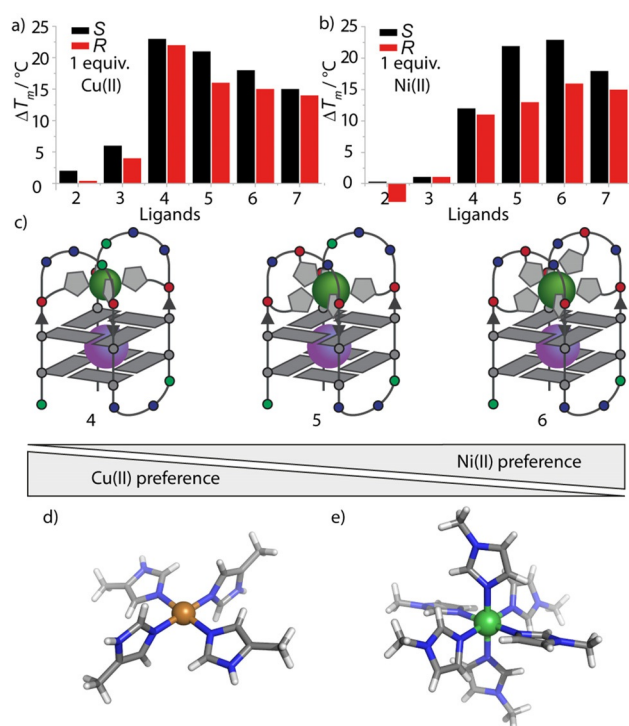
Knowing that only L^2 was able to complex transition-metal cations in unimolecular systems, the next question was whether an increase or decrease in the number of incorporated ligands would affect G-quadruplex topology and metal coordination. Therefore, sequences $htelL^{2R/S}_{2-7}$ with two-to-seven ligands were synthesized and investigated with respect to their folding topology and thermal stability. In $htelL^{2R/S}_2$ and $htelL^{2R/S}_3$, two or one ligands present in the parental sequence were replaced with thymine bases. TDS spectra revealed that both sequences $htelL^{2R/S}_2$ and $htelL^{2R/S}_3$ formed G-quadruplexes, but CD spectroscopy indicated a loss of the clear antiparallel conformation, presumably leading to mixtures of different topologies (Supporting Information, Figure S47). This prompted the design of two new sequences $htelL^{2R/S}_2B$ and $htelL^{2R/S}_3B$. In contrast to the previous sequences where the ligands were incorporated by replacing one of the G-tetrads, now all three G-tetrads were retained and instead thymine and adenine in the loop regions were replaced with L^2. Now, in NaCl a mainly antiparallel topology was observed for both sequences. In KCl, however, a signature was observed that either represents a hybrid 3+1 or a mix of topologies. Addition of Cu^{II} cations induced transformation into a pronounced antiparallel topology (Supporting Information, Figures S55 and S57). This sodium/potassium-dependent topology change was similarly reported for the unmodified htel sequence.[17] Considering that only in the antiparallel topology all ligands are arranged correctly (in opposite loops on one face of the G-quadruplex stack), subsequent studies with $htelL^{2R/S}_2B$ and $htelL^{2R/S}_3B$ were performed in sodium-containing buffers. Due to the additional G-tetrad for both sequences, high thermal stabilities with $T_m = 53\,°C$ ($htelL^{2S}_2B$) were observed. The addition of Cu^{II} cations to $htelL^{2S}_2B$ gave a weak thermal stabilization of $\Delta T_m = +2\,°C$ while for $htelL^{2S}_3B$ addition of Cu^{II} led to $\Delta T_m = +6\,°C$ and Zn^{II} $\Delta T_m = +2\,°C$. Furthermore, Cu^{II} addition induced a change of the CD signature to a more pronounced antiparallel topology, thus indicating the existence of a mixture of different topologies prior to copper complexation.[11]

Next, we increased the number of contained imidazole moieties to five, six and even seven by replacing adenines in the loop regions with L^2 in case of $htelL^{2R/S}_5$ and $htelL^{2R/S}_6$. For $htelL^{2R/S}_7$, an additional ligand was introduced into the loop, thus extending the overall sequence to 23 bases. TDS and CD spectroscopy supported the formation of G-quadruplexes in an antiparallel topology for all sequences, likewise to $htelL^{2R/S}_4$. Addition of Zn^{II} and Co^{II} to $htelL^{2S}_5$ showed weak thermal stabilizations $[\Delta T_m(Zn^{II}) = +4\,°C$, $\Delta T_m(Co^{II}) = +4\,°C]$ comparable to those observed for $htelL^{2S}_4$. More exciting were the observations made after addition of Ni^{II} and Cu^{II}. Although in the case of Cu^{II} ($\Delta T_m = +21\,°C$) the stabilization of $htelL^{2S}_5$ was lower compared to that of $htelL^{2S}_4$ ($\Delta T_m = +23\,°C$), the addition of Ni^{II} resulted in the exact opposite effect, showing a higher stabilization for $htelL^{2S}_5$ ($\Delta T_m = +22\,°C$) compared to $htelL^{2S}_4$ ($\Delta T_m = +12\,°C$).

This trend further continued with $htelL^{2S}_6$ showing an even lower thermal stabilization ($\Delta T_m = +18\,°C$) after Cu^{II} addition

compared to Ni^{II} ($\Delta T_m = +23\,^\circ$C). To explain these findings, a look at the preferred coordination environments of Cu^{II} and Ni^{II} is instructive. Cu^{II} is typically square-planar coordinated (with or without loosely bound water molecules in axial positions) as can be observed in reported crystal structures of Cu^{II} imidazole complexes (Figure 4d).[18] Ni^{II} exhibits a more versatile coordination chemistry with coordination numbers usually ranging from four to six. In the case of Ni^{II}-imidazole complexes, crystal structures are known in which six imidazole ligands are coordinated to the Ni^{II} cation in an octahedral fashion (Figure 4e).[18] The herein presented results nicely reflect the preferred coordination numbers of Cu^{II}, which is satisfied with four ligands, and Ni^{II}, which tends to be coordinated by six imidazole ligands. Hence, our system seems to allow for a selective fine-tuning of metal affinities by varying the number of introduced ligands (although it has to be mentioned that metal-mediated thermal stabilizations might not necessarily directly correspond to the underlying complexation constants). As expected, this trend abruptly stopped after incorporation of ligand number seven: Whereas Ni^{II} addition to htel$\mathbf{L^{2S}_7}$ ($\Delta T_m = +18\,^\circ$C) still caused a higher thermal stabilization compared to Cu^{II} ($\Delta T_m = +15\,^\circ$C), a drop of the thermal stabilization compared to htel$\mathbf{L^{2S}_6}$ was observed (see Figure 4). This could be a result of an overcrowded system in which more ligands are offered to Ni^{II} than it can coordinate.

In contrast to Cu^{II} and Ni^{II}, the results with Zn^{II} and Co^{II} were more complex. Although for htel$\mathbf{L^{2S}_4}$ only weak stabilizations were observed, addition of Zn^{II} and Co^{II} to htel$\mathbf{L^{2S}_6}$ resulted in a significant increase of the melting temperature [ΔT_m(Zn) = $+8\,^\circ$C, ΔT_m(Co) = $+8\,^\circ$C]. To explain the increased thermal stabilization for Zn^{II} two possible explanations were considered. Either Zn^{II} prefers the coordination of six imidazole ligands or four of the contained ligands in htel$\mathbf{L^{2S}_6}$ are better positioned to serve a tetrahedral coordination geometry. To clarify this, two new sequences called htel$\mathbf{L^2_4}$B and htel$\mathbf{L^2_4}$C, containing four ligands each in the differing loop positions, were synthesized (see Table 2 for sequences). In contrast to htel$\mathbf{L^2_4}$, two of the four ligands were placed in the loops and two close to the terminal G-tetrad, prearranging them in a tetrahedral geometry (Figure 5). Surprisingly, this change already led to significant higher thermal stabilities of htel$\mathbf{L^{2S}_4}$B ($T_m = 37\,^\circ$C) and htel$\mathbf{L^{2S}_4}$C ($T_m = 42\,^\circ$C) compared to htel$\mathbf{L^{2S}_4}$ ($T_m = 33\,^\circ$C) in the absence of transition metals, highlighting the crucial rule of the loop com-

Table 2. Sequences investigated in this study. Marked in red are the incorporated ligands (**L**).

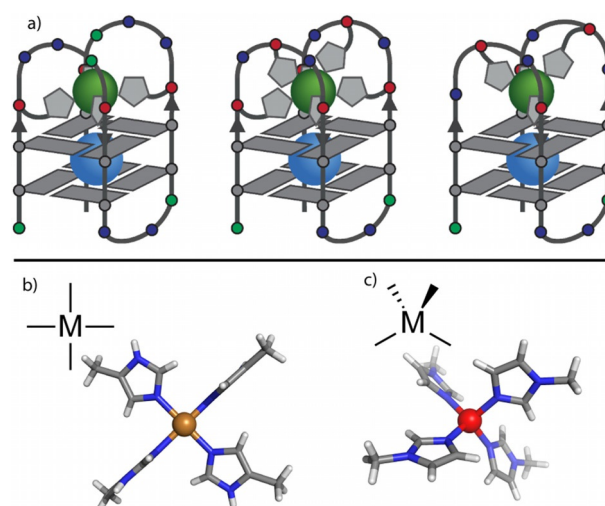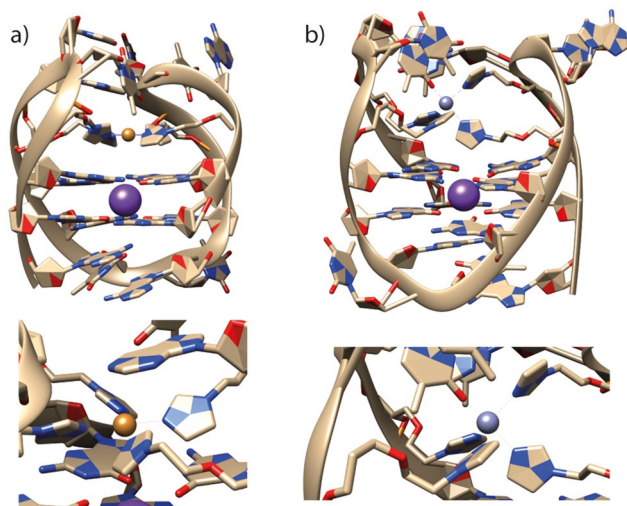|	Sequence 5′→3′
G$_4$L	LGG GG
G$_5$L	LGG GGG
htel	AGG GTT AGG GTT AGG GTT AGG G
htelL$_2$	AGG TTT ALG GTT AGG LTT ATG G
htelL$_2$B	AGG GTL TGG GTT AGG GTL TGG G
htelL$_3$	AGG LTT ALG GTT AGG LTT ATG G
htelL$_3$B	AGG GTL TGG GTT AGG GLT LGG G
htelL$_4$	AGG LTT ALG GTT AGG LTT ALG G
htelL$_4$B	AGG TLT LGG TTA GGL TLA GG
htelL$_4$C	AGG TLT LGG TTA GGT LTL GG
htelL$_5$	AGG LTL TLG GTT AGG LTT ALG G
htelL$_6$	AGG LTL TLG GTT AGG LTL TLG G
htelL$_7$	AGG LTL LTL GGT TAG GLT LTL GG

Figure 4. Fine-tuning of metal affinities. The bar diagrams in a) and b) display the changing G-quadruplex stabilizations after addition of Cu^{II} and Ni^{II} to htel$\mathbf{L^{2R/S}_{2-3}}$B and htel$\mathbf{L^{2R/S}_{4-7}}$. In a), decreasing Cu^{II}-mediated stabilization with an increase in ligand number from four to six is observed, whereas in b), the opposite effect is observed, that is, an increased stabilization from four to six ligands. c) Schematic illustration of the fine-tuning of Cu^{II} and Ni^{II} affinities. In d) and e), reported crystal structures of [Cu^{II}(4-methyl-imidazole)$_4$] and [Ni^{II}(N-methyl-imidazole)$_6$] complexes are shown.[18]

Figure 5. a) Schematic representation of the folded structures of htel$\mathbf{L_4}$, htel$\mathbf{L_6}$ and htel$\mathbf{L_4}$C. Reported X-ray structures of b) a square-planar [Cu^{II}(4-methyl-imidazole)$_4$] complex and c) a tetrahedral [Zn^{II}(N-methyl-imidazole)$_4$] complex.[18]

position on G-quadruplex stabilities. After addition of 1 equiv Zn^{II} to htelL^{2S}_4B ($\Delta T_m = +19\,°C$) and htelL^{2S}_4C ($T_m = +21\,°C$), indeed quite high thermal stabilizations were observed, unprecedented in the context of metal-mediated base pairs with Zn^{II}.[19] Interestingly, for Cu^{II} the opposite effect was observed, showing a lower thermal stabilization when added to htelL^{2S}_4C ($T_m = +21\,°C$) compared to htelL^{2S}_4 ($\Delta T_m = +23\,°C$; Supporting Information, Table S3). At first glance, this effect looks small, but it is remarkable considering the Irving–Williams series, according to which Cu^{II} usually shows higher complexation constants compared to those shown by Zn^{II}.[20] Considering that the number of imidazole ligands is constant in all three sequences, the changes in thermal stability can be assigned to the spatial arrangement of the ligands. This finding opens up a second layer of control besides varying the number of ligands to predesign coordination environments within folded G-quadruplexes to selectively suit a choice of metal cations and purposes.

To gain more detailed structural insights, MD simulations of htelL^{2S}_4 with bound Cu^{II} and Zn^{II} cations were prepared (Figure 6). Interestingly, although for Cu^{II} the expected square-planar coordination is observed, simulations with Zn^{II} show coordination of a fifth ligand, resulting in a trigonal-bipyramidal arrangement. As additional ligand, either a thymine residue from the loop region coordinating with its C4 carbonyl oxygen or a water molecule was observed. For further MD simulation data, including sequences htelL^{2S}_4C and htelL^{2S}_6 with and without bound Cu^{II} and Zn^{II} cations, see the Supporting Information.

tion-metal cations, such as Cu^{II}, Ni^{II}, Co^{II} and Zn^{II}, which was expressed by an increase in their thermal stability. The proposed metal complexes were investigated by native ESI-MS and trapped ion mobility spectrometry methods that turned out to be in accordance with folded G-quadruplex structures. In addition, MD simulations were performed to gain structural insights into the investigated systems, illustrate how metal coordination rigidifies the G-quadruplex structures and how ligand arrangement influences metal complexation. To show the robustness of the presented system, different counts of ligand L^2 (two to seven) were incorporated in unimolecular G-quadruplexes. Ligand number variation enabled the fine-tuning of metal affinities with respect to the typical coordination number. Thus Cu^{II}, usually coordinated by four ligands, showed the highest thermal stabilization after incorporation of four ligands in contrast to Ni^{II} or Co^{II}, which were found to prefer six ligands. In addition to the number of incorporated ligands, the system also enables the arrangement of ligands in certain geometries as shown for Zn^{II}, which prefers a tetrahedral arrangement, whereas Cu^{II} favors a square-planar binding site.

The herein introduced sophisticated control over the design of specific coordination environments inside cavities formed from folded DNA structures shows potential to facilitate the engineering of highly complex coordination spheres with metallo-enzyme-like activities. The simple phosphoramidite-based approach will allow for the expansion of the family of DNAzymes with members showing unprecedented functionality.[21] Our concept even allows to introduce an additional level of complexity by mixing different types of ligands, such as carboxylate or thiol groups, with the herein presented imidazole moieties, to create nonstatistical heteroleptic environments, a challenge that we are currently pursuing.

Acknowledgements

Conflict of interest

The authors declare no conflict of interest.

Figure 6. Representative pictures from MD simulations of htelL^{2S}_4 in complex with a) Cu^{II} and b) Zn^{II}.

Conclusions

The incorporation of two bioinspired imidazole ligandosides with chiral backbones into tetramolecular and unimolecular DNA G-quadruplex structures was established. We showed that the imidazole-modified systems fold in an antiparallel topology. The G-quadruplexes were found to complex various transi-

[1] a) J. A. Raven, M. C. W. Evans, R. E. Korb, *Photosynth. Res.* **1999**, *60*, 111; b) J. T. Rubino, K. J. Franz, *J. Inorg. Biochem.* **2012**, *107*, 129.

[2] a) R. H. Holm, P. Kennepohl, E. I. Solomon, *Chem. Rev.* **1996**, *96*, 2239; b) K. J. Waldron, J. C. Rutherford, D. Ford, N. J. Robinson, *Nature* **2009**, *460*, 823; c) K. Degtyarenko, *Bioinformatics* **2000**, *16*, 851.

[3] a) C. E. Valdez, Q. A. Smith, M. R. Nechay, A. N. Alexandrova, *Acc. Chem. Res.* **2014**, *47*, 3110; b) O. Yamauchi, A. Odani, M. Takani, *Dalton Trans.* **2002**, 3411.

[4] a) R. L. Shook, A. S. Borovik, *Inorg. Chem.* **2010**, *49*, 3646; b) H. M. Colquhoun, J. F. Stoddart, D. J. Williams, *Angew. Chem. Int. Ed. Engl.* **1986**, *25*, 487; *Angew. Chem.* **1986**, *98*, 483; c) A. J. Cornish, B. Ginovska, A. Thelen, J. C. S. da Silva, T. A. Soares, S. Raugei, M. Dupuis, W. J. Shaw, E. L. Hegg, *Biochemistry* **2016**, *55*, 3165; d) S. I. Mann, T. Heinisch, T. R. Ward, A. S. Borovik, *Chem. Commun.* **2018**, *54*, 4413; e) S. A. Cook, A. S. Borovik, *Acc. Chem. Res.* **2015**, *48*, 2407.

[5] a) E. Lo Presti, M. L. Perrone, L. Santagostini, L. Casella, E. Monzani, *Inorg. Chem.* **2019**, *58*, 7335; b) J. S. Kanady, E. Y. Tsui, M. W. Day, T. Agapie, *Science* **2011**, *333*, 733; c) D. Schilter, J. M. Camara, M. T. Huynh, S. Hammes-Schiffer, T. B. Rauchfuss, *Chem. Rev.* **2016**, *116*, 8693; d) K. D. Karlin, *Science* **1993**, *261*, 701; e) S. Piontek, K. Junge Puring, D. Siegmund, M. Smialkowski, I. Sinev, D. Tetzlaff, B. Roldan Cuenya, U.-P. Apfel, *Chem. Sci.* **2019**, *10*, 1075.

[6] a) Y. Lu, N. Yeung, N. Sieracki, N. M. Marshall, *Nature* **2009**, *460*, 855; b) S. Hirota, Y.-W. Lin, *J. Biol. Inorg. Chem.* **2018**, *23*, 7; c) A. Lombardi, C. M. Summa, S. Geremia, L. Randaccio, V. Pavone, W. F. DeGrado, *Proc. Natl. Acad. Sci. USA* **2000**, *97*, 6298; d) A. Hemschemeier, T. Happe, *Nat. Chem. Rev.* **2018**, *2*, 231; e) A. D. Liang, J. Serrano-Plana, R. L. Peterson, T. R. Ward, *Acc. Chem. Res.* **2019**, *52*, 585; f) J. Zhao, D. G. Bachmann, M. Lenz, D. G. Gillingham, T. R. Ward, *Catal. Sci. Technol.* **2018**, *8*, 2294; g) G. Roelfes, *Acc. Chem. Res.* **2019**, *52*, 545.

[7] a) Y. Xu, Y. Suzuki, T. Lönnberg, M. Komiyama, *J. Am. Chem. Soc.* **2009**, *131*, 2871; b) A. J. Boersma, B. L. Feringa, G. Roelfes, *Angew. Chem. Int. Ed.* **2009**, *48*, 3346; *Angew. Chem.* **2009**, *121*, 3396; c) S. Dey, C. L. Rühl, A. Jäschke, *Chem. Eur. J.* **2017**, *23*, 12162; d) M. Cheng, Y. Li, J. Zhou, G. Jia, S.-M. Lu, Y. Yang, C. Li, *Chem. Commun.* **2016**, *52*, 9644; e) A. J. Boersma, D. Coquière, D. Geerdink, F. Rosati, B. L. Feringa, G. Roelfes, *Nat. Chem.* **2010**, *2*, 991; f) D. Arian, L. Kovbasyuk, A. Mokhir, *Inorg. Chem.* **2011**, *50*, 12010; g) M. A. A. Garcia, Y. Hu, I. Willner, *Chem. Commun.* **2016**, *52*, 2153; h) S. Bandeira, J. Gonzalez-Garcia, E. Pensa, T. Albrecht, R. Vilar, *Angew. Chem. Int. Ed.* **2018**, *57*, 310; *Angew. Chem.* **2018**, *130*, 316.

[8] a) J. Müller, *Coord. Chem. Rev.* **2019**, *393*, 37; b) K. Tanaka, G. H. Clever, Y. Takezawa, Y. Yamada, C. Kaul, M. Shionoya, T. Carell, *Nat. Nanotechnol.* **2006**, *1*, 190; c) G. H. Clever, C. Kaul, T. Carell, *Angew. Chem. Int. Ed.* **2007**, *46*, 6226; *Angew. Chem.* **2007**, *119*, 6340; d) Y. Takezawa, M. Shionoya, *Acc. Chem. Res.* **2012**, *45*, 2066; e) H.-A. Wagenknecht, *Angew. Chem. Int. Ed.* **2003**, *42*, 3204; *Angew. Chem.* **2003**, *115*, 3322; f) A. Ono, H. Torigoe, Y. Tanaka, I. Okamoto, *Chem. Soc. Rev.* **2011**, *40*, 5855.

[9] a) K. Tanaka, Y. Yamada, M. Shionoya, *J. Am. Chem. Soc.* **2002**, *124*, 8802; b) M. A. Abdelhamid, L. Fábián, C. J. MacDonald, M. R. Cheesman, A. J. Gates, Z. A. Waller, *Nucleic Acids Res.* **2018**, *46*, 5886; c) D. M. Engelhard, R. Pievo, G. H. Clever, *Angew. Chem. Int. Ed.* **2013**, *52*, 12843; *Angew. Chem.* **2013**, *125*, 13078.

[10] a) R. Hänsel-Hertsch, M. Di Antonio, S. Balasubramanian, *Nat. Rev. Mol. Cell Biol.* **2017**, *18*, 279; b) S. Neidle, *Nat. Chem. Rev.* **2017**, *1*, 0041.

[11] a) D. M. Engelhard, J. Nowack, G. H. Clever, *Angew. Chem. Int. Ed.* **2017**, *56*, 11640; *Angew. Chem.* **2017**, *129*, 11799; b) D. M. Engelhard, A. Meyer, A. Berndhäuser, O. Schiemann, G. H. Clever, *Chem. Commun.* **2018**, *54*, 7455.

[12] a) P. M. Punt, G. H. Clever, *Chem. Sci.* **2019**, *10*, 2513; b) P. Röthlisberger, F. Levi-Acobas, I. Sarac, P. Marlière, P. Herdewijn, M. Hollenstein, *Org. Biomol. Chem.* **2017**, *15*, 4449.

[13] D. M. Engelhard, L. M. Stratmann, G. H. Clever, *Chem. Eur. J.* **2018**, *24*, 2117.

[14] Although a Co^{II} salt was used in this work, working under aerobic conditions might have resulted in at least partial oxidation to Co^{III}, indicated by the observation of slightly broadened ESI-MS isotopic patterns.

[15] a) M. J. Lecours, A. Marchand, A. Anwar, C. Guetta, W. S. Hopkins, V. Gabelica, *Biochim. Biophys. Acta.* **2017**, *1861*, 1353; b) A. Marchand, V. Gabelica, *J. Am. Soc. Mass Spectrom.* **2014**, *25*, 1146.

[16] V. D'Atri, M. Porrini, F. Rosu, V. Gabelica, *J. Mass Spectrom.* **2015**, *50*, 711.

[17] a) A. I. Karsisiotis, N. M. Hessari, E. Novellino, G. P. Spada, A. Randazzo, M. Webba da Silva, *Angew. Chem. Int. Ed.* **2011**, *50*, 10645; *Angew. Chem.* **2011**, *123*, 10833; b) P. L. T. Tran, J.-L. Mergny, P. Alberti, *Nucleic Acids Res.* **2011**, *39*, 3282; c) R. del Villar-Guerra, J. O. Trent, J. B. Chaires, *Angew. Chem. Int. Ed.* **2018**, *57*, 7171; *Angew. Chem.* **2018**, *130*, 7289.

[18] a) S. Godlewska, J. Jezierska, K. Baranowska, E. Augustin, A. Dołęga, *Polyhedron* **2013**, *65*, 288; b) W.-H. Wang, X.-Y. Su, Z.-H. Mao, J.-S. You, R.-G. Xie, *Acta Crystallogr. Sect. E* **2006**, *62*, m445; c) J. Reedijk, G. A. van Albada, B. Limburg, I. Mutikainen, U. Turpeinen, *Acta Crystallogr. Sect. E* **2012**, *68*, m90.

[19] B. Jash, J. Müller, *J. Inorg. Biochem.* **2018**, *186*, 301.

[20] H. Irving, R. J. P. Williams, *Nature* **1948**, *162*, 746.

[21] a) D. Morrison, M. Rothenbroker, Y. Li, *Small Methods* **2018**, *2*, 1700319; b) M. Hollenstein, *Molecules* **2015**, *20*, 20777; c) J. Wirmer-Bartoschek, H. Schwalbe, *Angew. Chem. Int. Ed.* **2016**, *55*, 5376; *Angew. Chem.* **2016**, *128*, 5462; d) A. Ponce-Salvatierra, K. Wawrzyniak-Turek, U. Steuerwald, C. Höbartner, V. Pena, *Nature* **2016**, *529*, 231; e) M. Hollenstein, C. Hipolito, C. Lam, D. Dietrich, D. M. Perrin, *Angew. Chem. Int. Ed.* **2008**, *47*, 4346; *Angew. Chem.* **2008**, *120*, 4418; f) H. Han, Q. Huang, H. Liu, J. Zhang, *ChemistrySelect* **2017**, *2*, 3925.